JOURNAL OF MATERIALS SCIENCE 30 (1995) 3415–3420

Photoelectrochemical behaviour of SnO_2 thin-film electrodes prepared by ultrasonic spray pyrolysis

KI HYUN YOON, DONG JIN NAM
Department of Ceramic Engineering, Yonsei University, Seoul, 120-749, Korea

Photoelectrochemical behaviour of the SnO_2 thin film prepared by ultrasonic spray pyrolysis was studied as a function of deposition time, annealing time and phosphorus content. The photocurrent increased up to 10 min (1.16 μm) with deposition time and then decreased. When the SnO_2 thin film was annealed for 10 min at 400 °C in air, the maximum value of photocurrent was obtained. When phosphorus was added to the SnO_2, photocurrent was decreased continuously with increasing phosphorus content.

1. Introduction

Ever since Fujishima and Honda proposed the possibility of the practical use of photoelectrochemical conversion using sunlight, many works in this area have been published, especially on the semiconducting electrode materials [1]. About 4.0–6.5 eV (190–310 nm) is needed to photoelectrolyse water directly. If the sunlight is used effectively, it is possible to split water into hydrogen and oxygen using photoelectrochemical conversion, because it requires only 1.23 eV to decompose electrochemically [2]. Some of the major factors affecting the efficiency of such electrode materials are a desirable band gap ($1.8\ eV < E_g < 2.5\ eV$), good chemical stability in aqueous electrolyte, and low electron affinity, etc. [3].

SnO_2 thin film has been used as an opto-electronic device [4] and as an electrode in solar cells [5] due to its high electrical conductivity, good optical transparency in visible light and good chemical stability in aqueous solution. Although SnO_2 thin film has a relatively large band gap (3.7 eV), because of increasing interest in hydrogen energy, its application in photoelectrochemical electrodes has been vigorously studied [6].

In this study, SnO_2 thin film was prepared by ultrasonic spray pyrolysis. It is possible to control the thickness of the film, and its electrical and optical properties easily. In particular, it can produce the film surface appropriate to a solar cell. Ultrasonic spray pyrolysis also has an economical advantage due to its high deposition rate, 1 nm min^{-1} [4].

The electrical photoelectrochemical properties of SnO_2 thin film prepared by ultrasonic spray pyrolysis as a function of its process parameters have been studied.

2. Experimental procedure

The sprayed solution was prepared from $SnCl_4$ (Junsei Chemical Co., Japan EP), deionized water and ethyl alcohol (Oriental Chemical Inc., Korea). HCl and PCl_5 (Fluka Chemie AG., Switzerland) were used as an additive and a dopant source, respectively. The concentrations of $SnCl_4$, C_2H_5OH, HCl and deionized water in the solution were fixed at 6, 30, 4 and 60 vol %, respectively. The Corning 7059 glasses (1.5 cm × 1.5 cm) were used as substrates to avoid charge compensation of alkali in an n-type semiconductor [6, 7]. Fig. 1 shows the basic construction of the ultrasonic spray pyrolysis equipment. This system consists of three parts: a mist generator, a deposition chamber and a fume scrubber to clean the exhausted gas and mist. Mist was generated by using the 1.6 MHz commercial ultrasonic vibrator. Air was used as a carrier gas and the oxygen source for oxidation. The substrate temperature was fixed at 300 °C. Annealing of the deposited film was conducted at 400 °C in air.

The thickness of the films was measured by ellipsometry (Auto EL IV, Rudolph Research International, USA), using as light source a He–Ne laser beam with the wavelength of 632.8 nm. The surface morphology of the film was observed by scanning electron microscopy (Hitachi S-800, Japan) with an electron beam source of the film-emission gun type. An X-ray diffractometer (Rigaku D-Max3, Japan) was also used for the crystallographical characterization at 30 kV, 10 mA. The elements in the films were analysed by Auger electron spectroscopy AES, Perkin–Elmer PHI 610). Electrical properties such as resistivity, concentration of carrier electrons and mobility of electrons, were measured by the Van der Pauw method [8]. The absorption coefficient of SnO_2 thin film was determined by measuring the transmittance using the UV-vis-NiR spectrophotometer (UV-vis-NiR spectrophotometer, Shimadzu UV-3100, Japan) from 200–800 nm, in the $\lambda > 305$ nm region using the 50 W tungsten–halogen lamp as a light source, and in the $\lambda \leq 305$ nm region using a deuterium lamp.

The photoelectrochemical behaviour of a SnO_2 thin film electrode was measured in 1N NaOH aqueous solution using the three-electrode PEC cell described by Yoon *et al.* [6, 9] with the SnO_2 photoanode, a platinum plate cathode and saturated calomel

0022–2461 © *1995 Chapman & Hall*

electrode (SCE) as the reference electrode. A 150 W halogen lamp (Philips, Germany) was used to illuminate the SnO_2 film electrode. The light was filtered through a 12 cm long water bath [10] and silica glass to reduce unwanted heat irradiation. The photocurrent–voltage characteristics were determined by measuring of the current difference between SnO_2 and the SCE. The scanning rate was 0.1 V min^{-1} with holding time of 30 s at every 1 V to obtain saturated photocurrent.

3. Results and discussion

The growth rate of the film deposited chemically is determined by such factors as temperature, flow rate, the concentration of the sprayed solution and deposition time. In this work, deposition time was the only variable parameter. Therefore, the thickness of the film was proportional to the deposition time. In Fig. 2 the linear proportionality of film thickness to deposition time is evident. It is in good agreement with the results reported by Maudes and Rodriguez [11]. The deposition rate was maintained at 2 nm s^{-1} during the overall deposition process. Fig. 2 also shows the columnar growth of the film [12].

Fig. 3 shows the results of X-ray diffraction of films with deposition time. As the deposition time increased, the orientation of the (2 0 0) peak was predominant [6, 13]. The (1 1 0) peak shown at the beginning of deposition, also disappeared with increasing deposition time. This particular directional orientation was caused by the tendency of film growth to reduce the surface energy. Fig. 4 shows the surface morphology of the film. Round crystallites grew compactly.

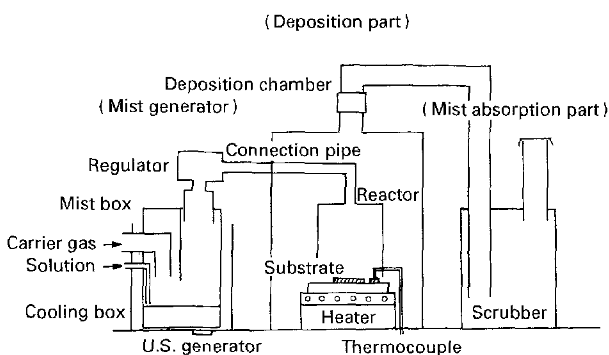

Figure 1 Basic construction of the ultrasonic spray pyrolysis equipment.

Fig. 5 shows AES analysis of SnO_2 thin film. Hambouleyron *et al.* [14] reported that residual chlorine exists in the film. In this study, the residual chlorine also appeared in the film.

Fig. 6 shows the variation of electrical properties of SnO_2 film with deposition time. Resistivity had a minimum value and the concentration of carrier electrons was maximum at 10 min deposition. After 10 min, the resistivity increased rapidly and carrier concentration decreased. When SnO_2 film was produced by thermal decomposition, oxygen vacancies donating carrier electrons appeared in the lattice. According to Vincent [15] it is possible to produce a controlled valence Sn^{4+}/Sn^{2+} in SnO_2

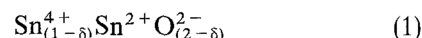

$$Sn^{4+}_{(1-\delta)}Sn^{2+}O^{2-}_{(2-\delta)} \quad (1)$$

and these oxygen vacancies donate two electrons

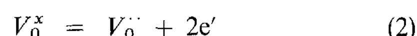

$$V_O^x = V_O^{\cdot\cdot} + 2e' \quad (2)$$

So the concentration of carrier electrons increased and resistivity decreased with an increase of deposition time in the early stages. However, after an optimum time (10 min), oxygen diffuses into the film from the surface and compensates the charge [16]. Thereby the resistivity increased rapidly and the concentration of carrier electrons decreased.

Fig. 7 shows the electrical properties of SnO_2 film with deposition time. As the annealing time increased, resistivity increased and carrier mobility increased slightly. However, the concentration of carrier electrons decreased rapidly. As mentioned above, SnO_2 thin film made by thermal decomposition has defects such as oxygen vacancies and residual impurities. Therefore, the concentration of Sn^{2+} which produces the donor level in the energy band gap is the major factor influencing the resistivity of SnO_2 thin film. This decrease in resistivity was due to the increase in concentration of donor electrons caused by residual impurities, such as alcohol or chlorine, which reduced Sn^{4+} to Sn^{2+} [17]. However, once these impurities were removed or when the film was annealed for a long time, Sn^{2+} was oxidized again. Thus the resistivity increased and donor concentration decreased. On the other hand, carrier mobility as a function of resistivity and carrier concentration increased slowly. It seems that the removal of residual impurities reduced the ionized impurity scattering in the lattice and the crystal growth reduced the grain-boundary scattering.

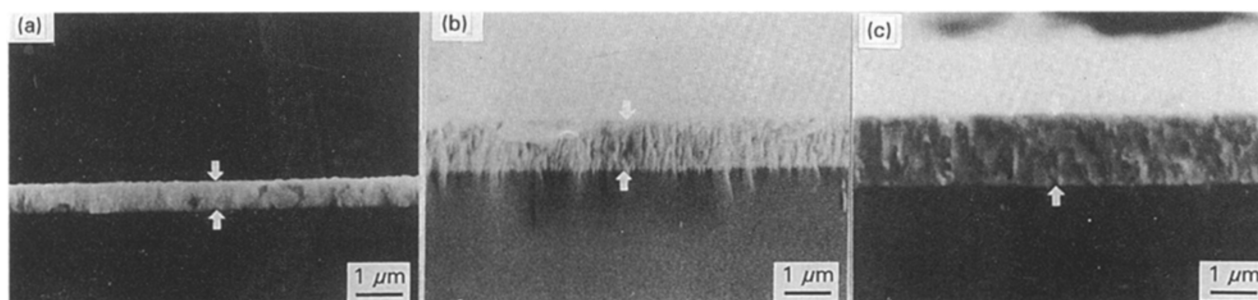

Figure 2 Changes in the cross-sectional surface of SnO_2 films with deposition time: (a) 5 min, (b) 10 min, (c) 15 min.

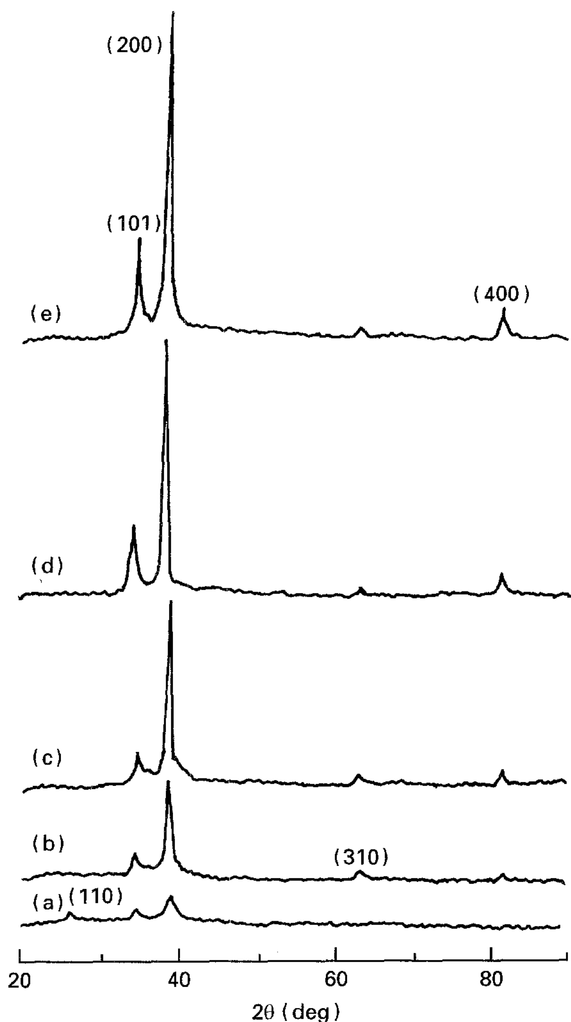

Figure 3 Change of the XRD pattern with deposition time: (a) 20 min, (b) 15 min, (c) 10 min, (d) 5 min, (e) 3 min.

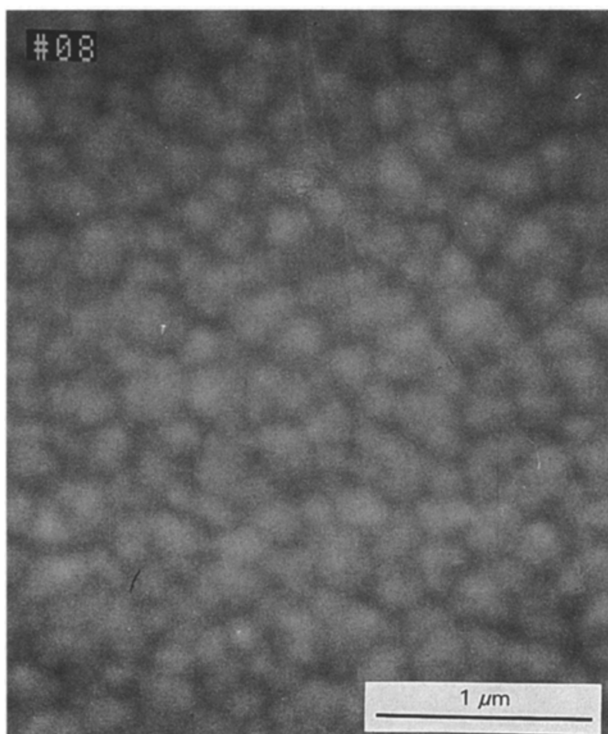

Figure 4 The surface structure of 15 min deposited SnO_2 film annealed in air at 400 °C, 10 min.

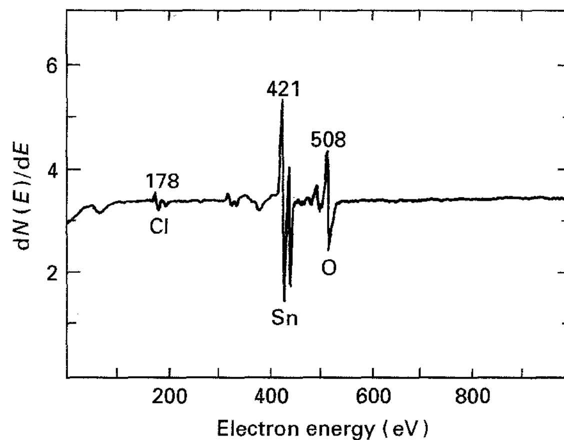

Figure 5 The AES spectrum of SnO_2 film after being sputtered for 5 min by Ar^+ ions. Deposition time 10 min, annealed for 10 min at 400 °C in air.

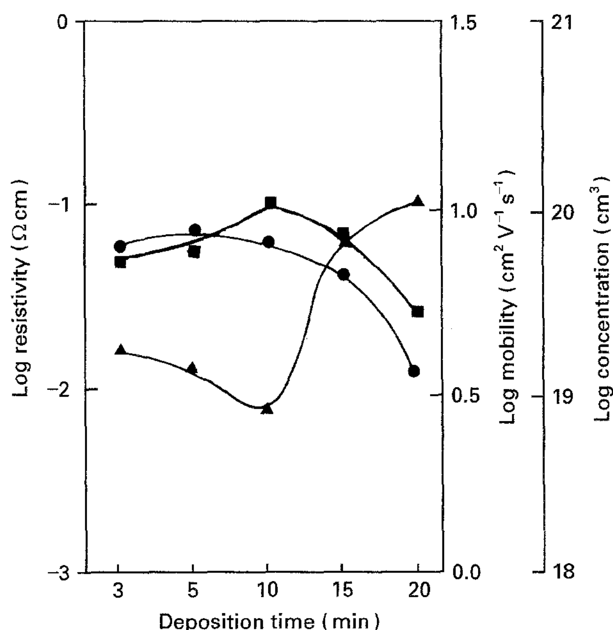

Figure 6 Variation of electrical properties of SnO_2 film with deposition time. Annealed in air at 400 °C, 10 min. (●) Carrier mobility, (■) carrier concentration, (▲) resistivity.

Fig. 8 shows the variation in the electrical properties of SnO_2 thin film with the addition of phosphorus. The carrier concentration increased on addition of phosphorus and was saturated after 3 wt % addition. Meanwhile, resistivity reached a minimum value at 3 wt % P doping. Carrier mobility varied slightly with phosphorus content. When phosphorus is added to SnO_2, it enters the lattice as a pentavalent ion [18]. The thermal energy excites the electrons from these ions into the crystal conduction band. The covalent model for semiconductors considers the phosphorus atoms to serve as donor atoms in SnO_2 film. Therefore, the addition of a small quantity of phosphorus to SnO_2 film decreased the resistivity by providing more donor atoms. However, further addition causes increasing stoichiometric deviation. This disorder in the lattice increases the effect of scattering mechanisms, such as phonon scattering and ionized impurity scattering, corresponding to the increment of resistivity.

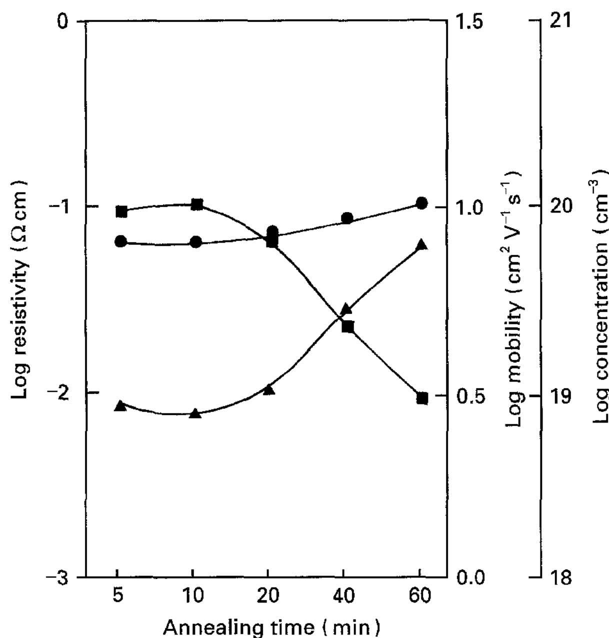

Figure 7 Variation of electrical properties of 10 min deposited SnO_2 film with annealing time. Annealed in air at 400 °C. (●) Carrier mobility, (■) carrier concentration, (▲) resistivity.

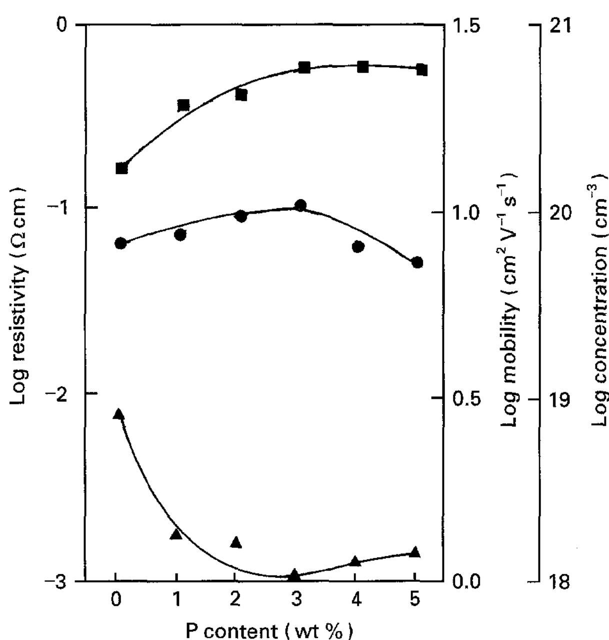

Figure 8 Variation of electrical properties of 10 min deposited SnO_2 film with phosphorus content. 10 min deposited, annealed in air at 400 °C, 10 min. (●) Carrier mobility, (■) carrier concentration, (▲) resistivity.

Therefore, it is certain that the heavily doped lattice can no longer be effective in producing phosphorus ions or in producing effective oxygen vacancies. The increment in mobility with a small addition of phosphorus is caused by a decrement in the grain-boundary potential due to an increase in the grain size as shown in Equation [17]

$$\mu = AT^{-1/2}\exp(-eV_B/kT) \qquad (3)$$

where V_B is the potential barrier for scattering at the grain boundary. At one point, after the concentration

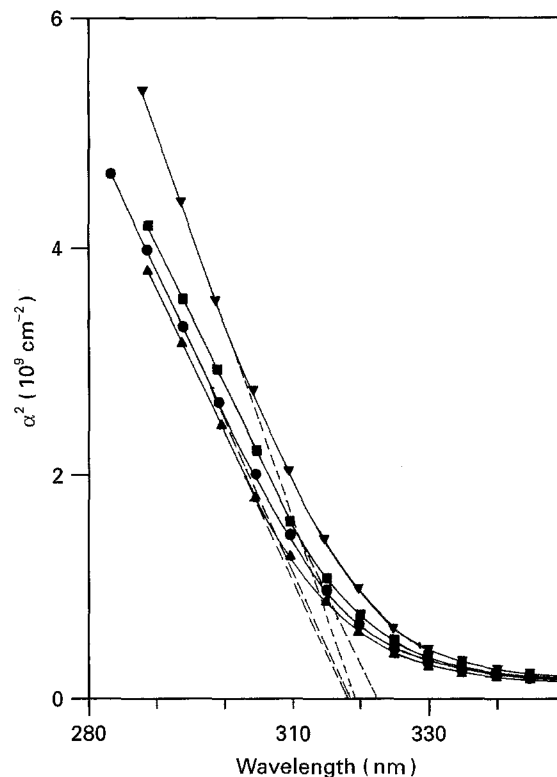

Figure 9 Variation of the square of the absorption coefficient, α^2, with wavelength for different deposition times: (▼) 5 min, (■) 10 min, (▲) 15 min, (●) 20 min.

of phosphorus reached the optimum value, the mobility decreased at higher doping concentration. It seems that clusters of segregated atoms at excess doping increase the grain-boundary potential.

Fig. 9 shows the square of absorption coefficient–optical band gap, E_g, curves with deposition time. The absorption coefficient was determined directly from the measurement of transmittance using Equation [19]

$$\alpha = (2.303/d)\log(1/T) \qquad (4)$$

where α is the film thickness. Optical band gap, E_g, is determined by extrapolating the linear portion of the α^2 versus wavelength plot to $\alpha = 0$. Up to 10 min, E_g moves to the longer wavelength region with deposition time, and after 10 min, it moves to the shorter wavelength region. It is known that the absorption of the thin film depends on the conductivity and deposition temperature of the film [20]. From Fig. 6, the lower the resistivity, the smaller is the optical band gap. In Fig. 10, the variation of E_g is similar to that with annealing time in Fig. 9. Therefore, the conductivity of SnO_2 thin film is the major factor of E_g. Fig. 11 shows the relationship between absorption coefficient and E_g with the doping concentration of phosphorus. E_g shifts to shorter wavelength with the phosphorus content. Shanthi *et al.* [21] reported the same phenomenon in the case of antimony doping. This shift in absorption edge can be attributed to the Moss–Burstein Shift [20, 21], which occurs owing to the filling of low-lying energy levels by the conduction electrons.

Fig. 12 shows the photocurrent–voltage curves for SnO_2 film electrodes with deposition time. The trends

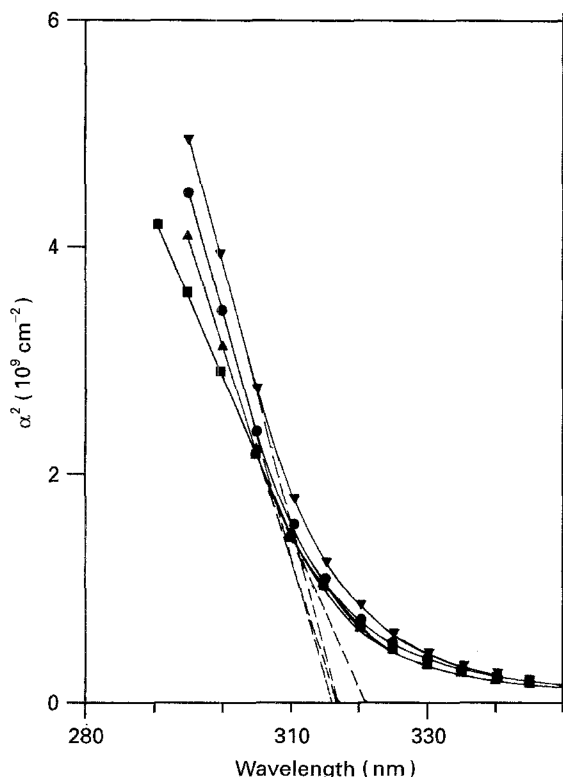

Figure 10 Variation of the square of the absorption coefficient, α^2, with wavelength for different annealing times: (▲) 5 min, (■) 10 min, (●) 20 min, (▼) 40 min.

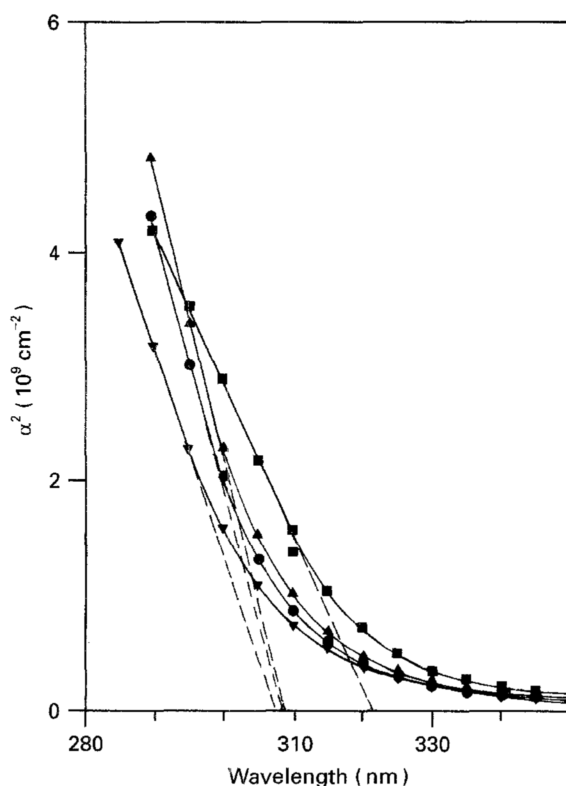

Figure 11 Variation of the square of the absorption coefficient, α^2, with wavelength for different phosphorus contents: (■) undoped, (▲) 1 wt % P, (▼) 3 wt % P, (●) 5 wt % P.

for the photocurrent to increase with deposition time were reversed at 10 min. On the basis of the Schottky barrier model [6, 22], the total current is the sum of the current due to excited electrons in the depletion

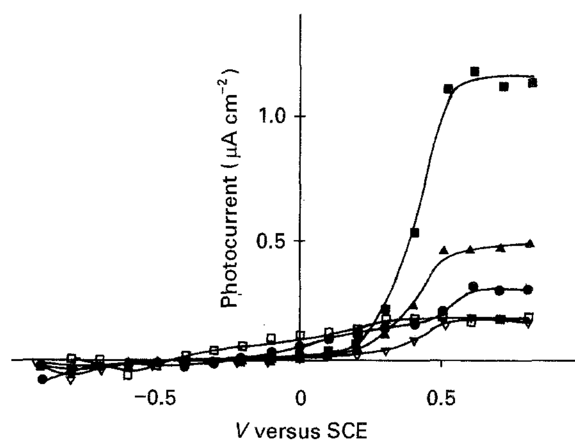

Figure 12 I–V curves in SnO_2 film electrodes with deposition time: (□) 3 min, (●) 5 min, (■) 10 min, (▲) 15 min, (▽) 20 min. annealed in air 400 °C, 10 min.

layer and the diffusion current in the bulk. The current due to excited electrons in the depletion layer is

$$J_{\text{depl}} = -q\phi[\exp(-\alpha W) - 1] \quad (5)$$

where q is the electron charge, ϕ the phonon flux, α the optical absorption coefficient. The depletion layer width is

$$W = \left(\frac{2\varepsilon\varepsilon_0}{qN_d}\right)^{1/2}(V - V_{fb})^{1/2} \quad (6)$$

where ε is the dielectric constant, ε_0 the permittivity of a vacuum, N_d the donor concentration, V the applied potential, and V_{fb} the flat band potential. The electric field in the depletion layer is

$$F = (V - V_{fb})/W \quad (7)$$

and the diffusion current in the bulk is

$$J_{\text{diff}} = q\phi\frac{\alpha L_p}{1 + \alpha L_p}\exp(-\alpha W) + qp_0\frac{D_p}{L_p} \quad (8)$$

where L_p is the hole diffusion length, D_p the hole diffusion coefficient and p_0 the hole concentration in the dark. In an n-type semiconductor with a wide band gap, for which p_0 can be neglected, the total current is

$$J = q\phi\left[1 - \frac{\exp(-\alpha W)}{1 + \alpha L_p}\right] \quad (9)$$

As shown in Fig. 6, with increasing deposition time, the concentration of carrier electrons and the carrier mobility increased up to 10 min, and then decreased. The electron concentration depends on the donor concentration. Therefore, from Fig. 6 and Equation 9, the depletion layer width can be expressed as a function of deposition time. Because the photocurrent is proportional to excited electrons in the depletion layer [22], the photocurrent must be minimum at 10 min deposition. However, from Fig. 9, the optical band gap, E_g, has a minimum value at 10 min deposition. Thus the excitation of electrons and the separation of an electron–hole pair are relatively easy. The voltage drop in the space charge layer is small due to the low

resistivity. So the recombination of the produced electron–hole pair is suppressed and the photocurrent increases.

Fig. 13 shows the photocurrent–voltage curves for SnO_2 film electrodes with annealing time. The photocurrent increased with increasing annealing time up to 10 min and decreased rapidly after 20 min. From Figs 7 and 10, the variation of E_g is in good agreement with the variation of resistivity and carrier concentration. That is, the oxygen vacancies which act as donors in the early stages are reduced and the carrier concentration decreased with increasing annealing time. After 10 min, the depletion layer is too wide and the electric field in the depletion layer is reduced. The concentration of carrier electrons decreases and the optical band gap shifts to a shorter wavelength (high energy). Therefore, the decrement of photocurrent is ascribed to the difficulty encountered in exciting electrons and in efficient separation of the electron–hole pair.

Fig. 14 shows the variation of photocurrent–voltage curve for SnO_2 film electrodes with phosphorus content. When phosphorus was added, the photocurrent decreased rapidly. As shown in Figs 8 and 11, with increasing phosphorus content, the concentration of carrier electrons and E_g increased. Meanwhile, the depletion layer width decreased. A decrease in photocurrent resulted from a too narrow depletion layer and a too small number of excited electrons. Thus, the effect of depletion layer on the photocurrent is greater than that of conductivity.

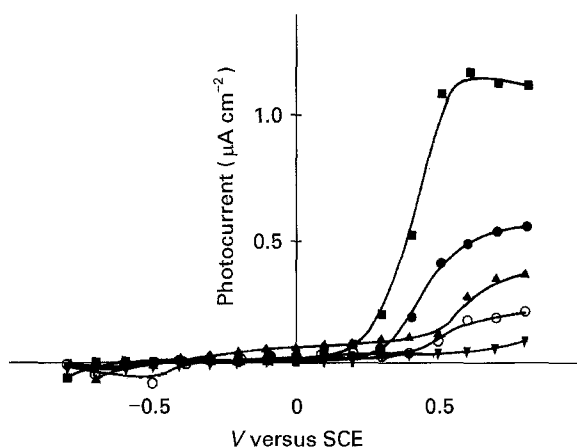

Figure 13 *I–V* curves in SnO_2 film electrodes with annealing time: (●) 5 min, (■) 10 min, (▲) 20 min, (○) 40 min, (▼) 60 min. 10 min deposited, annealed in air 400 °C.

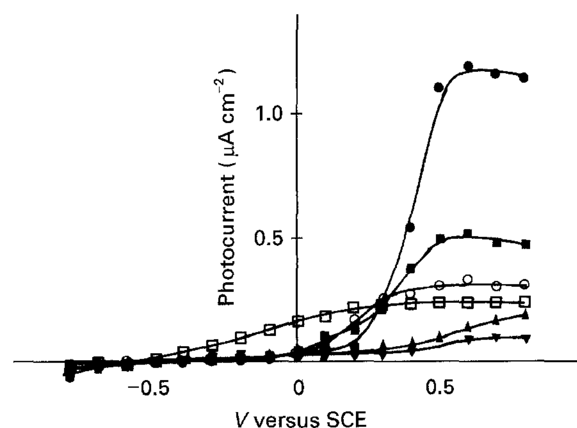

Figure 14 *I–V* curves in SnO_2 film electrodes with phosphorus content: (●) undoped, (■) 1 wt % P, (○) 2 wt % P, (□) 3 wt % P, (▲) 4 wt % P, (▼) 5 wt % P. 10 min deposited, annealed in air 400 °C, 10 min.

4. Conclusion

The thickness of film is linearly proportional to the deposition time. The deposition rate is $2\ nm\,s^{-1}$. As the deposition time increased the photocurrent increased up to 10 min (1.16 μm thickness) and then decreased. The photocurrent increased with increasing annealing time up to 10 min, and then decreased on further annealing. When phosphorus was added to SnO_2 film, the photocurrent decreased rapidly and did so continuously with further addition. Therefore, the photocurrent reaches a maximum value after 10 min deposition and annealing for 10 min at 400 °C in air.

Acknowledgement

This work was supported by the R and D Management Centre for Energy and Resources.

References

1. A. FUJISHIMA and K. HONDA, *Nature* **238** (7) (1972) 37.
2. M. S. WRIGHTON, A. B. ELLIS, P. T. WOLCZANSKI, D. L. MORSE, H. B. ABRAHAMSON and D. S. GIMLEY, *J. Am. Chem. Soc.* **98** (1976) 2774.
3. H. H. KUNG, H. S. JARRETT, A. W. SLEIGHT and A. FERRETTI, *J. Appl. Phys.* **48** (1977) 2463.
4. H. IIDA, T. MISHUKU, A. ITO, M. YAMANAKA and Y. HAYASHI, *Solar Energy Mater.* **17** (1988) 107.
5. T. H. UEN, K. F. HUANG, M. S. CHEN and Y. S. GOU, *Thin Solid Films* **158** (1988) 69.
6. T. H. KIM and K. H. YOON, *J. Appl. Phys.* **70** (1991) 2739.
7. H. KANEKO, *ibid.* **48** (1977) 1914.
8. S. M. SZE, "Physics of semiconductor devices" (Wiley, New York, 1981) p. 31.
9. K. H. YOON and C. H. KWON, *J. Appl. Phys.* **67** (1990) 868.
10. W. W. PUNN, Y. AIKAWA and A. J. BARD, *J. Electrochem. Soc.* **728** (1981) 222.
11. J. S. MAUDES and T. RODRIGUEZ, *Thin Solid Films* **69** (1980) 183.
12. H. HAITJEMA, J. PH. ELICH and C. J. HOOGENDOORN, *Solar Energy Mater.* **18** (1989) 283.
13. H. DEMIRYONT and K. E. NIETERING, *Solar Energy Mater.* **19** (1989) 79.
14. I. HAMBOULEYRON, C. CONSTANTINO and M. FANTINI, *ibid.* **9** (1983) 127.
15. COLIN A. VINCENT, *J. Electrochem. Soc.* **119** (1972) 515.
16. C. AGASHE, M. G. TAKWALE, B. R. MARATHE and V. G. BHIDE, *J. Mater. Sci.* **24** (1989) 2628.
17. T. YOKO, K. KAMIYA and S. SAKKA, *Yogyo-Kyokai-Shi* **95** (1987) 150.
18. J. P. PADHYAY, S. R. VISHWAKARMA and H. C. PRASAD, *Thin Solid Films* **169** (1989) 195.
19. WENDELL SPENCE, *J. Appl. Phys.* **38** (1967) 367.
20. K. B. SUNDARAM and G. K. BHAGAVAT, *J. Phys. D Appl. Phys.* **14** (1981) 533.
21. E. SHANTHI, V. DUTTA, A. BANERJEE and K. L. CHOPRA, *J. Appl. Phys.* **51** (1980) 6243.
22. M. A. BUTLER, *ibid* **48** (1977) 1912.

Received 28 April 1994
and accepted 20 January 1995